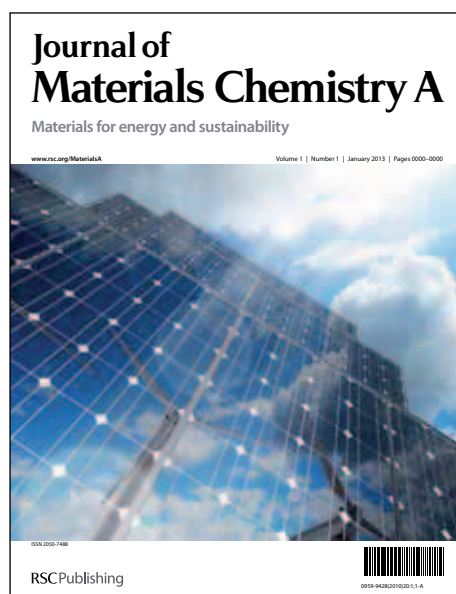


Journal of Materials Chemistry A

Accepted Manuscript



This is an *Accepted Manuscript*, which has been through the RSC Publishing peer review process and has been accepted for publication.

Accepted Manuscripts are published online shortly after acceptance, which is prior to technical editing, formatting and proof reading. This free service from RSC Publishing allows authors to make their results available to the community, in citable form, before publication of the edited article. This *Accepted Manuscript* will be replaced by the edited and formatted *Advance Article* as soon as this is available.

To cite this manuscript please use its permanent Digital Object Identifier (DOI®), which is identical for all formats of publication.

More information about *Accepted Manuscripts* can be found in the [Information for Authors](#).

Please note that technical editing may introduce minor changes to the text and/or graphics contained in the manuscript submitted by the author(s) which may alter content, and that the standard [Terms & Conditions](#) and the [ethical guidelines](#) that apply to the journal are still applicable. In no event shall the RSC be held responsible for any errors or omissions in these *Accepted Manuscript* manuscripts or any consequences arising from the use of any information contained in them.

Cite this: DOI: 10.1039/c0xx00000x

www.rsc.org/xxxxxx

ARTICLE TYPE

Development of MnO₂/porous carbon microspheres with partially graphitic structure for high performance supercapacitor electrode

Mingxian Liu, Lihua Gan,* Wei Xiong, Zijie Xu, Dazhang Zhu and Longwu Chen

Received (in XXX, XXX) Xth XXXXXXXXX 20XX, Accepted Xth XXXXXXXXX 20XX

DOI: 10.1039/b000000x

We report the development of MnO₂/porous carbon microspheres with partially graphitic structure for high performance supercapacitor electrode materials. Micro- and mesoporous carbon microspheres were fabricated based on a hydrothermal emulsion polymerization and common activation process. Manganese nitrate was introduced into the porosity of the carbon microspheres, followed by thermal treatment to transform into amorphous MnO₂. As-prepared MnO₂/porous carbon microspheres with high specific surface area (up to 1135 m² g⁻¹) and regular geometry (0.5–1.0 μm in diameter) benefit fast ion-transport and rapid charge–discharge, and contribute double-layer capacitance to the hybrid electrode. Besides, manganese dioxide shows high pseudocapacitive behaviour due to faradaic redox reaction. Furthermore, the introduction of MnO₂ greatly promotes the graphitization degree of the carbon matrix. A typical MnO₂/carbon sample shows partially graphitic structure with a very low intensity ratio of Raman D to G band ($I_D/I_G=0.27$), which substantially increases the electronic conductivity and reduces the internal resistance (decreased from 0.42 to 0.20 Ω). As a result, the MnO₂/porous carbon microspheres as supercapacitor electrode exhibit excellent electrochemical performance (459 F g⁻¹ at 1.0 A g⁻¹ and 354 F g⁻¹ at 20.0 A g⁻¹ in 6 M KOH electrolyte). The well-developed MnO₂/carbon hybrid materials with a high charge–discharge rate capability coupled with a high electrochemical capacitance highlights the great potential for widespread supercapacitor applications.

Introduction

During the past several decades, the global energy consumption has been accelerating at an alarming speed because of the fast worldwide economic expansion and population increase, and ever increasing human reliance on energy-based appliances.¹ As a result, developing green, highly efficient, and sustainable energy sources, as well as advanced technologies associated with energy conversion and storage becomes a very important work.² Due to their long cycle life, excellent pulse charge–discharge capability, environmental friendship and products safety, supercapacitors are a preferred choice in a wide range of applications, e.g., electric vehicles, short-term power sources for mobile electronic devices and other renewable energy storage systems.^{3–8} Generally, supercapacitors could be classified into electrical double layer capacitors and faradaic pseudo-capacitors on the basis of the energy storage mechanism. In electrical double layer capacitors, the capacitance comes from the pure electrostatic charge accumulated at the electrode/electrolyte interface;⁷ while in pseudo-capacitors, the energy is stored by a fast and reversible faradaic redox reaction in the electrode surface formed with electroactive materials, such as transition metal oxides and conducting polymers.^{9, 10} Carbon materials have been widely used in electrical double layer capacitor electrodes because of good electronic conductivity and chemical stability.¹¹ High-surface-area microporous carbons (e.g. activated carbons) exhibit high capability for charge accumulation at the electrode–electrolyte interface, which contributes to large capacitance.^{12, 13} While mesoporous carbons are favorable for high transportation speed of electrolyte ions, and

thus show better charge–discharge rates, especially under high loading current density.^{14–17} Besides, porous carbon microspheres with regular morphology and adjustable porosity and diameter can decrease the resistance of ion diffusion, and the package porosity among carbon spheres benefits the generation of ion buffer reservoirs and reduces ion diffusion distance.^{18–20} Thus, it is desirable to design and fabricate micro- and mesoporous carbon microspheres with regular geometry and well-developed pore structure for tailoring high performance electrodes to be used in electrical double layer capacitors.¹⁹ On the other hand, various transition metal oxides, such as RuO₂, MnO₂, IrO₂, NiO, Co₂O₃, etc., show good capacitive properties and are considered as suitable electrode materials for faradaic pseudo-capacitors.^{21–25} Among these materials, amorphous hydrated ruthenium oxide is one of the most attractive candidates for the electrodes of electrochemical capacitors because of ideal pseudocapacitive behavior, high specific capacitance and excellent reversibility.¹⁰ Unfortunately, high cost causes much difficulty in the development of RuO₂ as commercial acceptable electrodes for faradaic pseudo-capacitors. MnO₂ is one of the most promising substitute due to its low cost, low toxicity coupled with high specific capacitance (ca. 1110 F g⁻¹).^{26–29}

Each type of electrode materials has its merits and demerits. Generally, carbon materials show high power density and long cycle life, but have low electrochemical capacitance.³⁰ While transition metal oxides offer higher energy density than carbon materials and better cycling stability than polymer materials, but suffer a drawback of poor conductivity.²⁵ Considering this and the aspects mentioned above, it has inspired efforts to develop hybrid of transition metal oxides (e.g. MnO₂) and porous carbons (e.g. micro- and mesoporous carbon microspheres). In this case,

the electrode shows combined advantages of carbon and MnO₂ materials, and double-layer capacitance and pseudocapacitance contribute indivisible to the total electrochemical capacitance value of a supercapacitor. Such hybrid thus represents promising and innovative materials, and is supposed to be a preferable choice for supercapacitor electrode.

Emulsion is a dispersion system which generally comprises emulsifier and at least two phases, a water phase and an oil phase.³¹ Emulsion polymerization is usually adopted to fabricate some commercially important polymers such as poly(vinyl chloride).^{32,33} Recently, this method has been widely used for the synthesis of porous or spherical polymer (and carbon).³⁴⁻³⁷ In this work, we demonstrate the design and fabrication of partially graphitic MnO₂/micro- and mesoporous carbon microspheres (denoted as MnO₂/carbon) for high performance supercapacitor electrode. Micrometer-scaled carbon spheres with micro- and mesopores were synthesized *via* a hydrothermal emulsion polymerization and activation process. MnO₂ was introduced into the porosity of carbon microspheres by using manganese nitrate as the precursor. High-surface-area porous carbon microspheres are beneficial for fast ion-transport and rapid charge-discharge, and provide double-layer capacitance to the hybrid electrode. While MnO₂ embedded in the carbon matrix exhibits high pseudocapacitive properties. Besides, the presence of MnO₂ greatly promotes the graphitization degree of the carbons, which brings excellent electronic conductivity and very low internal resistance. A typical MnO₂/carbon hybrid as supercapacitor electrode exhibits a high charge-discharge rate capability coupled with a high specific capacitance (459 F g⁻¹ at 1.0 A g⁻¹ and 354 F g⁻¹ at 20.0 A g⁻¹ in 6 M KOH electrolyte). Therefore, we believe that the well-designed MnO₂/carbon composite materials with excellent electrochemical performance offer promising prospects for supercapacitor applications.

Experimental section

Materials

Liquid paraffin ($\rho = 0.84 \text{ g cm}^{-3}$), Span 80, Tween 80, resorcinol, formaldehyde aqueous solution (37–40 wt.%), KOH, ethanol and Mn(NO₃)₂ were analytical reagents and were purchased from Sinopharm Chemical Reagent Co. Ltd. Graphite was supplied by Shanghai Colloid Chemical Plant. Polytetrafluoroethylene (PTFE, catalog number FR301B) was purchased from Shanghai 3F New Materials Co., Ltd. Nickel foil was manufactured by Shanghai Hongxiang Plant. High pure nitrogen was offered by Shanghai BOC Special Gases Sales Service Co., Ltd. All materials were used as they received without any further purification. Water used was distilled water.

Synthesis of MnO₂/porous carbon microspheres

An oil-in-water (O/W) emulsion system was fabricated similarly according to the procedure described in our previous reported work.^{19,38} The mass ratio of Span 80, Tween 80, liquid paraffin, resorcinol, formaldehyde and water is 1:1.33:4.17:3.88:5.04:2.08. Liquid paraffin acts as the oil phase, resorcinol, formaldehyde and water serves as an aqueous phase, and Span 80/Tween 80 takes the role of emulsifier. When the aqueous phase was added slowly into the oil phase contained emulsifiers under stirring, an

O/W emulsion was obtained. This emulsion was heated to 200 °C for 5 h in an autoclave to synthesize resorcinol/formaldehyde polymer microspheres, followed by drying and carbonization (1000 °C) with a heating rate of 5 °C min⁻¹ in high pure nitrogen atmosphere to prepare mesoporous carbon microspheres. Micropores were generated in the carbon microspheres by further KOH activation (KOH: carbon=1:3, w/w) at 850 °C (5 °C min⁻¹) in N₂ flow.¹⁹ Manganese nitrate-ethanol solution was mixed with the micro- and mesoporous carbon microspheres for about 24 h at room temperature (The mass percentage of Mn(NO₃)₂ to the porous carbon microspheres was 2–10%), followed by natural evaporation of the ethanol. The sample was heated to 900 °C (5 °C min⁻¹) under pure nitrogen flow to fabricate MnO₂/carbon (denoted as MnO₂(x%)/carbon in which x% represents the mass percentage of manganese nitrate to porous carbon microspheres, and the porous carbon microspheres without MnO₂ was denoted as MnO₂(0%)/carbon).

Characterization

Scanning electron microscopy (SEM) observation of the MnO₂/carbon sample was done on a Hitachi S-4800 equipment. Nitrogen adsorption and desorption analysis was conducted on a Micromeritics Tristar 3000 analyzer. The adsorption data was taken at -196 °C to calculate the specific surface area by the Brunauer-Emmett-Teller (BET) model, and the adsorption branch was used in the calculation of pore size distribution by Barrett-Joyner-Halenda (BJH) model. Raman spectrum analysis was carried out by using Renishaw Invia system, under $\lambda_{\text{exc}} = 514 \text{ nm}$ laser excitation. Powder X-ray diffraction (XRD) test was carried out on a Bruker D8 equipment with Cu K α ($\lambda = 0.154056 \text{ nm}$) radiation. X-ray photoelectron spectroscopy (XPS) was done on a Kratos AXIS Ultra DLD system.

Electrochemical Measurements

Electrochemical measurements were estimated via a conventional three-electrode system in a 6 M KOH electrolyte solution, which was performed on a CHI660D electrochemical workstation. Hg/HgO electrode was used as a reference electrode, and nickel foam as a counter electrode. The working electrode was prepared by pressing the mixture of MnO₂/carbon, graphite and PTFE with a mass ratio of 8:1:1 between two pieces of Ni foam under 30 MPa. Then 1.0 mm thick circle electrode (with a diameter of ~1.2 cm) was dried overnight at 100 °C (the total mass of an electrode is ~10 mg). The electrochemical properties were tested by cyclic voltammogram and galvanostatic charge-discharge (the potential window in the range of -1.0 to 0 V versus Hg/HgO electrode), and electrochemical impedance spectroscopy (frequency range between 1 mHz and 10³ kHz). The electrochemical capacitance of the electrode was determined as follow:

$$C_m = \frac{C}{m} = \frac{I \times \Delta t}{m \times \Delta V} \quad (1)$$

in which C_m is specific capacitance (F g⁻¹), C is capacitance (F), m is the mass of electrode (g), I is the charge-discharge current (A), Δt is the discharge time (s), and ΔV is the potential window of the charge-discharge (V).

Results and discussion

Fig. 1 shows SEM photographs of a representative MnO₂/carbon sample. The MnO₂/carbon has regular spherical geometry with diameters of 0.5–1.0 μm, as shown in Fig. 1A. When the aqueous phase (resorcinol–formaldehyde–water) was added into the oil phase (liquid paraffin) contained emulsifiers (Span 80–Tween 80) under stirring, an O/W emulsion was manufactured. Without hydrothermal condition, the polymerization of the O/W emulsion in presence of NaOH and the following carbonization led to the formation of monolithic carbon foams with pore size of 2–3 μm.³⁸ However, a completely different kind of carbon material, carbon microspheres, was prepared by the hydrothermal polymerization and carbonization of the emulsion with the same composition. The carbon microspheres show similar dimension compared with the pore sizes of our previous reported porous carbons. Based on the geometry of the resultant carbons, it could be concluded that the O/W emulsion does not maintain its droplet structure under hydrothermal condition. The generation of spherical carbon instead of monolithic one corresponds to a result of a water-in-oil (W/O) type emulsion polymerization.^{19, 39} In general, many factors such as hydrophile-lipophile balance value, phase inversion temperature, oil/aqueous phase level, component ratio, monomer properties, and additive could influenced the emulsion properties,^{31, 40, 41} and one could achieve a phase inversion by varying these factors. When the original O/W emulsion was transferred into an autoclave (200 °C), the system temperature and pressure increases, inducing a phase inversion to a W/O emulsion and leading to the generation of carbon microspheres. In addition, the carbon microspheres consist of nanoscaled carbon particles (Fig. 1B). The porosity among these nanoparticles is very useful for the introduction of manganese precursor into the inside of the porous carbon microspheres, and it also benefits the homogenous dispersity of manganese oxide in the carbon matrix and promotes the formation of MnO₂/carbon complex.

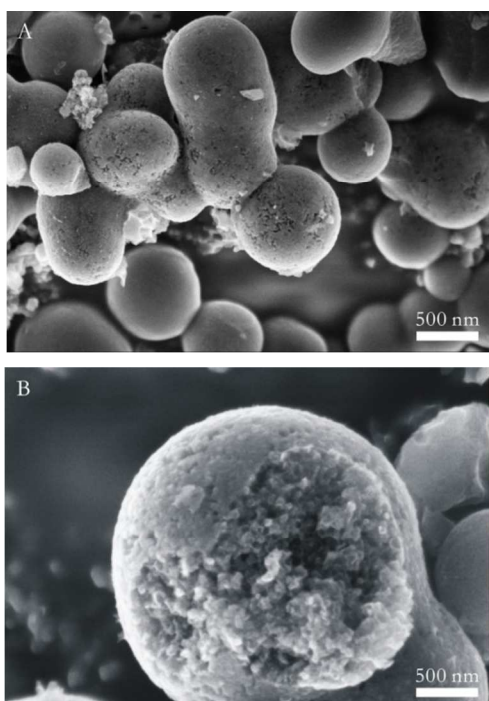


Fig. 1 SEM photographs of a representative MnO₂/carbon sample.

Fig. 2A shows XRD patterns of MnO₂/carbon samples. In pure porous carbon microspheres (MnO₂(0%)/carbon), there are two broad diffraction peaks located at about 2θ=24° and 43° which correspond to the (002) and (100) lattice planes of amorphous carbon. These peaks become sharp and narrow in MnO₂/carbon samples, especially in MnO₂(5%)/carbon. Besides, it causes much difficulty to observe the weak diffraction peaks of MnO₂ because of low content. To indicate the presence of manganese oxide in MnO₂/carbon (e.g., MnO₂(5%)/carbon), XPS measurement were conducted. However, the atomic ratio for Mn/C is too low to be detected (The mass percentage of manganese nitrate to porous carbon microspheres in MnO₂(5%)/carbon sample is 5%. After decomposition, the theoretical MnO₂ content is about 2.43%, and the theoretical atomic ratio for Mn/C is less than 0.4%). The mass percentage of MnO₂ is 2.26% in MnO₂(5%)/carbon measured by removing the carbon under air condition in a Muffle furnace, which is similar with the calculated value of manganese oxide in the sample. Manganese nitrate was decomposed to manganese dioxide after heat treatment. It can be concluded from Fig. 2 that the introduction of MnO₂ into amorphous carbon matrix could improve its microcrystalline structure and increase its graphitization degree. Graphitization is a process involving the transformation of metastable nongraphitic carbon into graphitic one. Catalytic pyrolysis of carbon precursors with the aid of various elements is one of the widely used strategies to fabricate graphitic or partially graphitic carbons.^{42–45} For example, our group previously achieved the graphitization of aerogel-like carbons in molten sodium metal.⁴² Increasing the graphitization degree of porous carbons preserving as far as possible their high surface areas and pore volumes, are of special interest in electrode materials due to their efficient electronic conductivity and excellent mass transport.⁴⁶

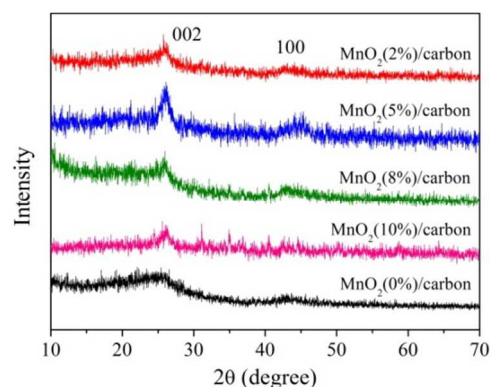


Fig. 2 XRD patterns of MnO₂/carbon samples.

Fig. 3 shows Raman spectra of MnO₂/carbon samples. MnO₂(0%)/carbon has a distinct pair of bands located at 1360 cm⁻¹ (D band) and 1584 cm⁻¹ (G band). The Raman D peak is a typical feature for disordered graphite or crystal defects; while the Raman G peak is an ideal graphitic lattice vibration mode with E_{2g} symmetry.⁴⁷ The Raman spectra of MnO₂/carbon samples, compared with pure carbon microspheres, have similar intensity of the D and G peaks, but show the appearance of G' band (~2700 cm⁻¹) which is a typical characteristic of undisturbed or highly ordered graphitic lattices. MnO₂(5%)/carbon exhibits a very sharp G' peak, suggesting the generation of graphitic domains.⁴² In addition, MnO₂(5%)/carbon, compared with other MnO₂/carbon

samples, shows new or more distinguished Raman peaks located at $\sim 2450\text{ cm}^{-1}$, $\sim 2940\text{ cm}^{-1}$ (D+G model) and $\sim 3240\text{ cm}^{-1}$ (2D' or G* model) which were observed in highly oriented pyrolytic graphite.^{48, 49} Therefore, the presence of these peaks also indicate the microcrystalline structure of MnO₂(5%)/carbon was improved. The ratio of the relative intensity of D peak and G peak (I_D/I_G) denotes the degree of graphitization, defects or the domain size of graphitization.⁴⁶ Generally, the graphitization degree is in inverse ratio to the I_D/I_G value. MnO₂(0%)/carbon, MnO₂(2%)/carbon, MnO₂(8%)/carbon, and MnO₂(10%)/carbon have the I_D/I_G values of 0.99, 0.96, 1.08 and 0.99, respectively. However, the I_D/I_G value for MnO₂(5%)/carbon sample is as low as 0.27, indicating the amorphous carbon matrix can be partially transformed to crystalline ones in case of suitable amount of manganese oxide.

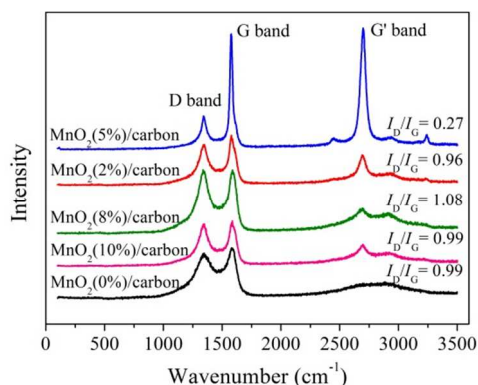


Fig. 3 Raman spectra of MnO₂/carbon samples.

Fig. 4 exhibits nitrogen adsorption and desorption isotherms of MnO₂/carbon. All samples are found to be of type IV isotherm curves with obvious hysteresis loops at relative pressure P/P_0 of 0.45–1.0, which is a feature of capillary condensation occurred in mesoporous solids. All MnO₂/carbon samples show pore sizes of about 4.0 nm (Table 1). Except emulsifiers, Span 80 and/or Tween 80 serve as a soft template during hydrothermal condition. We were previously synthesized mesoporous carbons with pore sizes of 4.0 nm by using Span 80 as template.⁵⁰ MnO₂/carbon samples have specific surface areas of 916–1135 $\text{m}^2\text{ g}^{-1}$ and total pore volume of 0.77–1.03 $\text{cm}^3\text{ g}^{-1}$. The micro- and mesopores benefits the introduction of MnO₂ into the carbon matrix and promotes the formation of hybrid MnO₂/carbon. On the one hand, the similar BET areas and pore volume among these samples indicate that the porous structure of carbon microspheres has been well kept. High surface areas are retained after the MnO₂ insertion. On the other hand, as a result of the increased graphitization degree and improved microcrystalline structure in the presence of MnO₂, the BET areas and the pore volume of MnO₂/carbon (e.g. MnO₂(2%)/carbon or MnO₂(5%)/carbon) are somewhat increased. However, these parameters decrease in case of large amount MnO₂, suggesting the blockage of some pores.

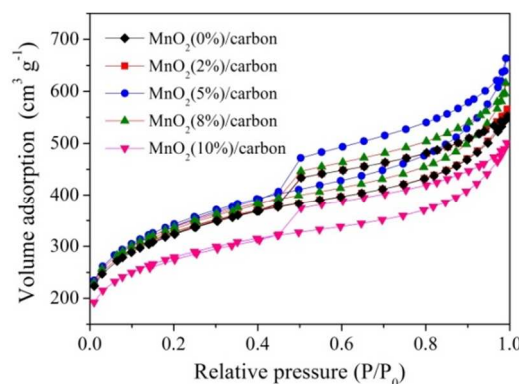


Fig. 4 N₂ adsorption and desorption isotherms of MnO₂/carbon.

Table 1. Pore parameters of MnO₂/carbon^a

sample	S_{BET} ($\text{m}^2\text{ g}^{-1}$)	S_{mi}^b ($\text{m}^2\text{ g}^{-1}$)	S_{me}^b ($\text{m}^2\text{ g}^{-1}$)	P (nm)	V_t ($\text{cm}^3\text{ g}^{-1}$)
MnO ₂ (0%)/carbon	1010	522	488	4.0	0.85
MnO ₂ (2%)/carbon	1073	344	729	4.0	0.87
MnO ₂ (5%)/carbon	1135	304	831	4.0	1.03
MnO ₂ (8%)/carbon	1110	339	771	3.9	0.95
MnO ₂ (10%)/carbon	916	299	617	3.9	0.77

^a S_{BET} , specific surface area; S_{mi} , micropore surface area; S_{me} , mesopore surface area; P , pore size; V_t , the total pore volume; ^bThe data of micropore surface area and mesopore surface area was obtained by nitrogen adsorption and desorption report.

Electrochemical impedance spectroscopy was conducted to understand the conductive and diffusive behavior of MnO₂/carbon electrodes. Fig. 5 shows the Nyquist plots of MnO₂/carbon electrodes in 6 M KOH solution, all of which consists of a quasi-semicircle, an vertical line and an almost 45 degree diagonal line. The existence of vertical line reveals good electrochemical capacitive properties of MnO₂/carbon electrodes, while the 45° line denotes the feature of ion diffusion into the carbon electrodes. At high frequency, the diameter of the semicircle corresponds to polarization resistance or charge transfer resistance of the electrode. Pure carbon electrode (MnO₂(0%)/carbon) with good conductivity shows smaller charge transfer resistance than other MnO₂/carbon samples. When the imaginary part tends to zero, the value of the real part reveals the internal resistance of electrode which comprises the electrolyte resistance, the intrinsic resistance of the active material, and the contact resistance between interfacial active material and current collector.¹⁹ Because the same electrolyte, current collector and assembling technique for electrode were used during the test, the intercept shown in the high frequency semicircle essentially reveals the conductivity of the active materials (MnO₂/carbon complex). The internal resistance of MnO₂(5%)/carbon electrode is as low as 0.20 Ω , much lower than that of MnO₂(0%)/carbon (0.42 Ω). The improved conductivity of MnO₂(5%)/carbon is attributed to its increased graphitization degree and improved microcrystalline structure. As a comparison, MnO₂(10%)/carbon sample shows a similar internal resistance (0.43 Ω) with pure porous carbon microspheres electrode.

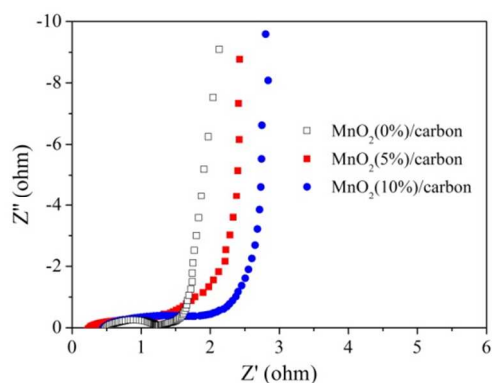


Fig. 5 Nyquist plots of MnO₂/carbon electrodes in 6 M KOH solution.

Fig. 6A shows the cyclic voltammograms of MnO₂/carbon electrodes at a scan rate of 10 mV s⁻¹ in 6 M KOH electrolyte. At low scan rate, MnO₂(2%)/carbon and MnO₂(5%)/carbon electrodes show quasi-rectangular shapes at a potential window ranging from 0 to -1.0 V, suggesting an ideal capacitive behavior. The absence of oxidation and reduction peaks in the MnO₂(2%)/carbon and MnO₂(5%)/carbon electrodes suggests that the supercapacitor is charged–discharged at a pseudoconstant rate over the complete voltammetric cycles.^{51, 52} In case of higher dosage of manganese oxide, the obtained hybrid electrode (MnO₂(8%)/carbon or MnO₂(10%)/carbon) exhibits redox peaks, which corresponds to the reversible faradaic redox reaction in the electrode surface formed with electroactive materials of MnO₂. The redox peaks of MnO₂(10%)/carbon is weaker than those of MnO₂(8%)/carbon. This because only the surface or surface layer of MnO₂ responds to the pseudo capacitance. In case of relatively high content of MnO₂, the manganese oxide aggregate in the carbons, i.e., MnO₂(10%)/carbon, which leads to (a) the blockage of some pores (as shown in Table 1 and corresponding discussion) and (b) decreased utilization rate of the MnO₂ surface. Therefore, MnO₂(10%)/carbon electrode shows weaker redox peaks in the cyclic voltammogram compared with MnO₂(8%)/carbon. Among MnO₂/carbon electrodes, MnO₂(5%)/carbon shows the highest integrated area in the cyclic voltammograms. Generally, the larger the integrated area is, the higher the electrochemical capacitance is. Therefore, MnO₂(5%)/carbon electrode shows better electrochemical performance as a result of improved microstructure and increased graphitization degree. Besides, the cyclic voltammograms are obviously distorted with increasing potential scan rate, such as mesoporous carbon microsphere electrode operated at 100 mV s⁻¹ or above,¹⁹ which could be ascribed mainly to the limited ion incorporation into the active electrode, i.e., only the outer surface or subsurface is utilized for charge storage.^{52, 53} In contrast, the cyclic voltammogram of MnO₂(5%)/carbon electrode still retains a rectangular-like shape even at 200 mV s⁻¹, as shown in Fig. 6B. This indicates good accessibility of the ions to the electrochemically active surface, and the excellent capacitive behavior of the electrode in quick charge–discharge operations.⁴⁶ The MnO₂(5%)/carbon electrode could provide more electron/ion paths and faster transport of these charge carriers due to increased graphitization degree and improved electron conductivity, resulting in swift and reversible redox reactions and rectangular cyclic voltammograms.

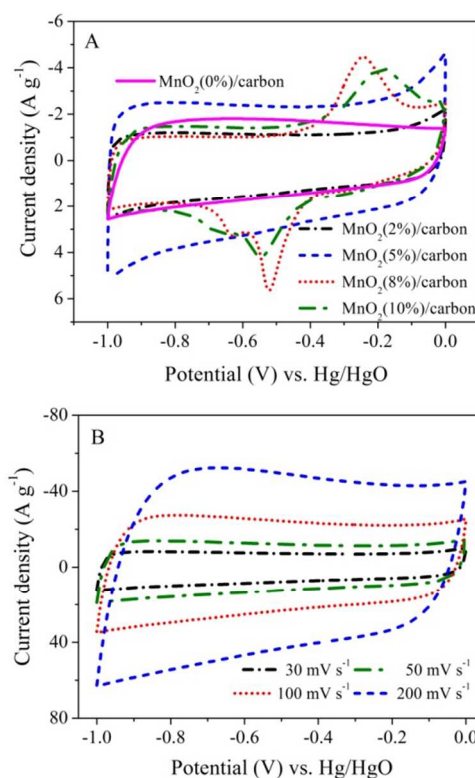


Fig. 6 Cyclic voltammograms of (A) MnO₂/carbon electrodes at 10 mV s⁻¹ and (B) MnO₂(5%)/carbon electrode at 30, 50, 100 and 200 mV s⁻¹ in 6 M KOH electrolyte solution.

Fig. 7A show the galvanostatic charge–discharge profiles of MnO₂/carbon electrodes at a loading current density of 1.0 A g⁻¹ in 6 M KOH solution. Basically, these curves are linear and symmetric, suggesting high coulombic efficiency and good reversibility. The discharge curves of MnO₂/carbon electrodes are somewhat distorted, and there is a galvanostatic charge–discharge plateau in MnO₂(8%)/carbon electrode, which is an indication of pseudocapacitance of manganese dioxide. The change law of the galvanostatic charge–discharge curves among the MnO₂/carbon (as well as the reason) is something like that of cyclic voltammogram (Fig. 6A). The charge–discharge time of MnO₂(5%)/carbon electrode was significantly increased compared with other MnO₂/carbon electrodes at the same current density, indicating that MnO₂(5%)/carbon electrode provides a much larger charge capacity. This result is consistent with that of the cyclic voltammograms. The electrochemical capacitances of MnO₂/carbon electrodes calculated with eq 1 were shown in Table 2. The specific capacitance of MnO₂(5%)/carbon electrode is as high as 459 F g⁻¹ at 1.0 A g⁻¹, much higher than that of MnO₂(0%)/carbon (171 F g⁻¹), MnO₂(2%)/carbon (156 F g⁻¹), MnO₂(8%)/carbon (288 F g⁻¹), and MnO₂(10%)/carbon (207 F g⁻¹). Fig. 7B show galvanostatic charge–discharge curves of MnO₂(5%)/carbon electrode under different current densities. The potential–time profiles still maintain a triangle shape at high current densities, such as 10 and 20.0 A g⁻¹, implying that MnO₂(5%)/carbon electrode is suitable for application in supercapacitors in which rapid charge–discharge is required. MnO₂(5%)/carbon electrode exhibits a specific capacitance of 367 F g⁻¹ at 10.0 A g⁻¹ and 354 F g⁻¹ at a high current density of 20.0 A g⁻¹. Compared with pure micro- and mesoporous carbon

microspheres, MnO₂/carbon electrodes show enhanced specific capacitance as a result of pseudocapacitance of MnO₂. Moreover, MnO₂(5%)/carbon possesses partially graphitic structure and low internal resistance among the MnO₂/carbon samples, which endows the electrode much higher capacitance, as shown in Table 2. Besides, as we have discussed, the aggregation of manganese oxide resulting from relatively high doping content would bring pore blockage as well as decreased surface utilization rate of MnO₂. This could reduce the ion transport speed and decrease the electrochemical capacitance. Therefore, considering all aspects discussed above, MnO₂(5%)/carbon is an optimum sample for supercapacitor electrode application. To evaluate the cycle stability of MnO₂(5%)/carbon electrode, we used cyclic voltammetry (at a scan rate of 10 mV s⁻¹) to characterize the long-term charge–discharge behavior. The specific capacitance of MnO₂(5%)/carbon electrode retains ~90% (414 F g⁻¹) of the original capacity up to 1000 cycles at 1.0 A g⁻¹, as shown in Fig. 8, suggesting good electrochemical cycle stability.

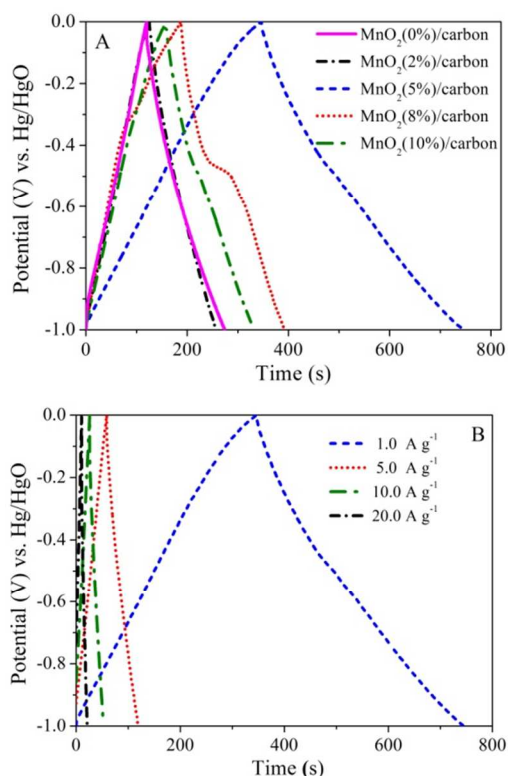


Fig. 7 Galvanostatic charge–discharge curves of MnO₂/carbon electrodes at 1.0 A g⁻¹ (A), and MnO₂(5%)/carbon electrode at 1.0, 5.0, 10.0 and 20.0 A g⁻¹ (B) in 6 M KOH electrolyte solution.

Table 2. Specific capacitances of MnO₂/carbon electrodes under different loading current densities.

sample	Specific capacitances (F g ⁻¹)			
	1.0 A g ⁻¹	5.0 A g ⁻¹	10.0 A g ⁻¹	20.0 A g ⁻¹
MnO ₂ (0%)/carbon	171	163	157	-
MnO ₂ (2%)/carbon	156	132	116	103
MnO ₂ (5%)/carbon	459	392	367	354
MnO ₂ (8%)/carbon	288	245	224	206
MnO ₂ (10%)/carbon	207	183	176	168

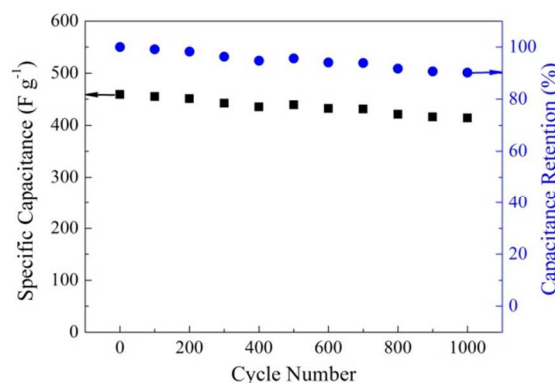
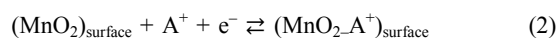


Fig. 8 Long-term cycle stability of MnO₂(5%)/carbon electrode at 1.0 A g⁻¹ in 6 M KOH electrolyte solution.

Presently, the most plausible elementary processes associated with the capacitive behavior of amorphous MnO₂ involving alkali metal ion (A⁺) electrolyte could be described as follows:^{54,55}



Thus, rapid K⁺ intercalation/deintercalation and swift electron transfer are essential to achieve fast, reversible surface redox reactions. Although the theoretical capacity of MnO₂ is up to 1110 F g⁻¹,²⁶ its actual capacity is usually much lower than that value because only the surface or surface layer of MnO₂ responds to the pseudo capacitance. For example, Li et al. described the fabrication of flexible graphene/MnO₂ composite papers for supercapacitor electrode, the capacitance of the composite with the MnO₂ weight ratio of 24% was 256 F g⁻¹ at 0.5 A g⁻¹.⁵⁶ Chen et al. prepared a composite of graphene oxide supported by needle-like MnO₂ nanocrystals. The resultant hybrid electrode had a electrochemical capacitance of 111 F g⁻¹ at 1.0 A g⁻¹.⁵⁷ Hierarchical manganese oxide/carbon nanocomposites reported by Peng et al. was 156 F g⁻¹ at 2.0 A g⁻¹.⁵⁸ Compared with the above MnO₂ based electrode materials, our MnO₂/carbon with well-designed microstructure and morphology substantially increases conductivity and markedly reduces the internal resistance, resulting in excellent electrochemical performance. Besides, MnO₂(5%)/carbon electrode shows much higher electrochemical capacitance than those of mesoporous carbon microspheres (~170 F g⁻¹),⁵⁹ carbon nanocages (178 F g⁻¹),⁶⁰ and graphene (205 F g⁻¹) at 10 A g⁻¹,⁶¹ and 3D hierarchical porous graphitic carbon (170 F g⁻¹)⁴⁵, carbon nanotubes/hollow carbon spheres (150 F g⁻¹)⁶² at 20.0 A g⁻¹, as well as most other carbon electrodes under the same current density. Therefore, the MnO₂/carbon with high-rate electrochemical performance shows promising prospects in supercapacitor applications.

Conclusions

In conclusion, partially graphitic MnO₂/micro- and mesoporous carbon microspheres were fabricated by using a hydrothermal emulsion polymerization and activation process, followed by introduction of MnO₂ into the porosity of carbon microspheres. High-surface-area porous carbon microspheres benefit fast ion-transport and rapid charge–discharge, and provide double-layer capacitance to the hybrid electrode. While MnO₂ embedded in the carbon matrix bring pseudocapacitance. On the other hand, the graphitization degree of the carbon matrix was greatly increased in the presence of MnO₂, leading to excellent conductivity and low internal resistance. Consequently, the binary MnO₂/carbon hybrid materials as supercapacitor electrode show excellent high-

rate electrochemical performance associated with a high specific capacitance (459 F g^{-1} at 1.0 A g^{-1} and 354 F g^{-1} at 20.0 A g^{-1} in 6 M KOH electrolyte). We believe that the well-designed and high-performance $\text{MnO}_2/\text{carbon}$ composite material provides new opportunities for a wide range of energy storage applications.

Acknowledgments

This work was financially supported by the National Natural Science Foundation of China (20973127, 21207099, 21273162), the Science and Technology Commission of Shanghai Municipality, China (11nm0501000, 12ZR1451100), and Key Subject of Shanghai Municipal Education Commission (J50102).

Notes and references

Department of Chemistry, Tongji University, 1239 Siping Road, Shanghai 200092, P. R. China. Fax: 86 21 65981097; Tel: 86 21 65982654-8430; E-mail: ganlh@tongji.edu.cn

† Electronic Supplementary Information (ESI) available. See DOI: 10.1039/b000000x/

- 1 L. Dai, D.W. Chang, J.-B. Baek and W. Lu, *Small*, 2012, **8**, 1130.
- 2 G. Wang, L. Zhang and J. Zhang, *Chem. Soc. Rev.*, 2012, **41**, 797.
- 3 Y. G. Wang, H. Q. Li and Y. Y. Xia, *Adv. Mater.*, 2006, **18**, 2619.
- 4 R. Liu and S. B. Lee, *J. Am. Chem. Soc.*, 2008, **130**, 2942.
- 5 X. Du, C. Wang, M. Chen, Y. Jiao and J. Wang, *J. Phys. Chem. C*, 2009, **113**, 2643.
- 6 O. Barbieri, M. Hahn, A. Herzog and R. Kötz, *Carbon*, 2005, **43**, 1303.
- 7 L. Zhang and X. Zhao, *Chem. Soc. Rev.* 2009, **38**, 2520.
- 8 C. Xu, J. Sun and L. Gao, *J. Mater. Chem.*, 2011, **21**, 11253.
- 9 J.-K. Chang, M.-T. Lee, W.-T. Tsai, M.-J. Deng, H.-F. Cheng and I.-W. Sun, *Langmuir*, 2009, **25**, 11955.
- 10 X. Dong, W. Shen, J. Gu, L. Xiong, Y. Zhu, H. Li and J. Shi, *J. Phys. Chem. B*, 2006, **110**, 6015.
- 11 Z. Lei, N. Christov, L. L. Zhang and X. S. Zhao, *J. Mater. Chem.*, 2011, **21**, 2274.
- 12 J. Qian, M. Liu, L. Gan, P. K. Tripathi, D. Zhu, Z. Xu, Z. Hao, L. Chen and D. S. Wright, *Chem. Commun.*, 2013, **49**, 3043.
- 13 L. Zhang, F. Zhang, X. Yang, K. Leng, Y. Huang and Y. Chen, *Small*, 2013, **9**, 1342.
- 14 W. M. Qiao, Y. Song, S. H. Hong, S. Y. Lim, S.-H. Yoon, Y. Korai and I. Mochida, *Langmuir*, 2006, **22**, 3791.
- 15 T. Morishita, Y. Soneda, T. Tsumura and M. Inagaki, *Carbon*, 2006, **44**, 2360.
- 16 H. Jiang, J. Ma, C. Li, *Adv. Mater.*, 2012, **24**, 4197.
- 17 Y. Lv, L. Gan, M. Liu, W. Xiong, Z. Xu, D. Zhu and D.S. Wright, *J. Power Sources*, 2012, **209**, 152.
- 18 H. Kim, M. E. Fortunato, H. Xu, J. H. Bang and K. S. Suslick, *J. Phys. Chem. C*, 2011, **115**, 20481.
- 19 W. Xiong, M. Liu, L. Gan, Y. Lv, Y. Li, L. Yang, Z. Xu, Z. Hao, H. Liu and L. Chen, *J. Power Sources*, 2011, **196**, 10461.
- 20 M. Liu, L. Gan, W. Xiong, F. Zhao, X. Fan, D. Zhu, Z. Xu, Z. Hao and L. Chen, *Energy Fuels* 2013, **27**, 1168.
- 21 M. Nakayama, A. Tanaka and Y. Sato, *Langmuir*, 2005, **21**, 5907.
- 22 X. Wu, Y. Zeng, H. Gao, J. Su, J. Liu and Z. Zhu, *J. Mater. Chem. A*, 2013, **1**, 469.
- 23 G. Q. Zhang, L. Yu, H. E. Hoster, X. W. Lou, *Nanoscale*, 2013, **5**, 877.
- 24 L. Demarconay, E. Raymundo-Pinero and F. Béguin, *J. Power Sources*, 2011, **196**, 580.
- 25 H. Jiang, P. S. Lee and C. Li, *Energy Environ. Sci.*, 2013, **6**, 41.
- 26 Q. Liao, N. Li, H. Cui and C. Wang, *J. Mater. Chem. A*, 2013, **1**, 13715.
- 27 J. Jiang and A. Kucernak, *Electrochim. Acta*, 2002, **47**, 2381.
- 28 Y. Peng, Z. Chen, J. Wen, Q. Xiao, D. Weng, S. He, H. Geng and Y. Lu, *Nano Res.*, 2011, **4**, 216.
- 29 W. Wei, X. Cui, W. Chen and D. G. Ivey, *Chem. Soc. Rev.*, 2011, **40**, 1697.
- 30 W. Xing, C. C. Huang, S. P. Zhuo, X. Yuan, G. Q. Wang, D. Hulicova-Jurcakova, Z. F. Yan and G. Q. Lu, *Carbon*, 2009, **47**, 1715.
- 31 L. Chen, Y. Shang, H. Liu and Y. Hu, *J. Colloid Interface Sci.*, 2006, **301**, 644.
- 32 P. V. Smallwood, *Polymer*, 1986, **27**, 1609.
- 33 J. Wieme, M.-F. Reyniers and G. B. Marin, *Macromolecules*, 2009, **42**, 7797.
- 34 E. B. Mock and C. F. Zukoski, *Langmuir*, 2010, **26**, 13747.
- 35 A. Menner, R. Powell and A. Bismarck, *Macromolecules*, 2006, **39**, 2034.
- 36 E. Groison, S. Brusseau, F. D'Agosto, S. Magnet, R. Inoubli, L. Couvreur and B. Charleux, *ACS Macro Lett.*, 2012, **1**, 47.
- 37 F. Wang, G. Xu, Z. Zhang and X. Xin, *Eur. J. Inorg. Chem.*, 2006, 109.
- 38 M. Liu, L. Gan, F. Zhao, H. Xu, X. Fan, C. Tian, X. Wang, Z. Xu, Z. Hao and L. Chen, *Carbon*, 2007, **45**, 2710.
- 39 M. Liu, L. Gan, Z. Xu, L. Chen, J. Hu and H. Liu, *Chem. Lett.*, 2010, **39**, 274.
- 40 D. Morales, J. M. Gutiérrez, M. J. García-Celma and Y. C. Solans, *Langmuir*, 2003, **19**, 7196.
- 41 A. Barbetta, N. R. Cameron and S. J. Cooper, *Chem. Commun.*, 2000, 221.
- 42 Z. Xu, B. Xia, W. Wang, T. Ji, C. Ma and L. Gan, *Carbon*, 2011, **49**, 3385.
- 43 A. B. Fuertes and T. A. Centeno, *J. Mater. Chem.*, 2005, **15**, 1079.
- 44 S. Yi, Z. Fan, C. Wu and J. Chen, *Carbon*, 2008, **46**, 378.
- 45 D.-W. Wang, F. Li, M. Liu, G. Q. Lu and H.-M. Cheng, *Angew. Chem. Int. Ed.*, 2008, **47**, 373.
- 46 W. Gao, Y. Wan, Y. Dou and D. Zhao, *Adv. Energy Mater.*, 2011, **1**, 115.
- 47 A. Sadezky, H. Muckenhuber, H. Grothe, R. Niessner and U. Poßschl, *Carbon*, 2005, **43**, 1731.
- 48 P. Tan, Y. Deng and Q. Zhao, *Phys. Rev. B*, 1998, **58**, 5435.
- 49 A.C. Ferrari and J. Robertson (Ed.), *Raman Spectroscopy in Carbons: from Nanotubes to Diamond*. The Royal Society, London, 2004.
- 50 M. Liu, L. Gan, C. Tian, J. Zhu, Z. Xu, Z. Hao and L. Chen, *Carbon*, 2007, **45**, 3045.
- 51 X. Y. Lang, A. Hirata, T. Fujita and M. W. Chen, *Nat. Nanotechnol.*, 2011, **6**, 232.
- 52 L. Yang, S. Cheng, Y. Ding, X. Zhu, Z. L. Wang and Liu M. *Nano Lett.*, 2011, **12**, 321.
- 53 L. H. Bao, J. F. Zang and X. D. Li, *Nano Lett.*, 2011, **11**, 1215.
- 54 S. C. Pang, M. A. Anderson and T. W. Chapman, *J. Electrochem. Soc.*, 2000, **147**, 444.
- 55 V. Subramanian, H. Zhu, R. Vajtai, P. M. Ajayan and B. Wei, *J. Phys. Chem. B*, 2005, **109**, 20207.
- 56 Z. Li, Y. Mi, X. Liu, S. Liu, S. Yang and J. Wang, *J. Mater. Chem.*, 2011, **21**, 14706.
- 57 S. Chen, J. Zhu, X. Wu, Q. Han and X. Wang, *ACS Nano*, 2010, **4**, 2822.
- 58 Y. Peng, Z. Chen, J. Wen, Q. Xiao, D. Weng, S. He, H. Geng and Y. Lu, *Nano Res.*, 2011, **4**, 216.
- 59 Q. Li, R. Jiang, Y. Dou, Z. Wu, T. Huang, D. Feng, J. Yang, A. Yu and D. Zhao, *Carbon*, 2011, **49**, 1248.
- 60 K. Xie, X. Qin, X. Wang, Y. Wang, H. Tao, Q. Wu, L. Yang and Z. Hu, *Adv. Mater.*, 2012, **24**, 347.
- 61 Y. Wang, Z. Q. Shi, Y. Huang, Y. F. Ma, C. Y. Wang, M. M. Chen and Y. S. Chen, *J. Phys. Chem. C*, 2009, **113**, 13103.
- 62 Q. Wang, J. Yan, Y. Wang, G. Ning, Z. Fan, T. Wei, J. Cheng, M. Zhang and X. Jing, *Carbon*, 2013, **52**, 20.

Graphical Abstract

Development of MnO₂/porous carbon microspheres with partially graphitic structure for high performance supercapacitor electrode

Mingxian Liu, Lihua Gan,* Wei Xiong, Zijie Xu, Dazhang Zhu and Longwu Chen

MnO₂/porous carbon microspheres with partially graphitic structure were designed and synthesized for high performance supercapacitor electrode materials.

